The International Journal of Advanced Manufacturing Technology (2020) 106:4375–4389
https://doi.org/10.1007/s00170-019-04917-2

ORIGINAL ARTICLE

Feasibility study in combined direct metal deposition (DMD) and plasma transfer arc welding (PTA) additive manufacturing

M. Dalaee[1,2] · F. Cheaitani[3] · A. Arabi-Hashemi[4] · C. Rohrer[4] · B. Weisse[4] · C. Leinenbach[4] · K. Wegener[1]

Received: 7 October 2019 / Accepted: 30 December 2019 / Published online: 16 January 2020

Abstract
Direct metal deposition (DMD) and plasma transfer arc welding (PTA) are two metal deposition techniques, which are well-known for high-quality and high-productivity level of fabrication, respectively. In the field of additive manufacturing (AM) of large-scale metallic parts, combined technologies of these methods can offer advantageous solutions to manufacture complex parts with the industry's economical requirements of productivity and energy efficiency. To study the feasibility of a combined DMD–PTA technique, a preliminary analysis in the specification of both techniques is conducted. Hybrid layers are fabricated using stainless steel EN X3CrNiMo13-4. Joining strategy of dissimilar layers, as well as microstructure and tensile strength of the hybrid layers, are examined. A comparison of the PTA and DMD process specifications shows both PTA and DMD processes are capable of being integrated into one operating system to enhance productivity. Layer-wise deposition of both processes presents a dense microstructure between dissimilar layers. However, side-by-side deposition of PTA and DMD layers requires proper joint-strategy due to higher heat input and wider and thicker deposited track in the regular current PTA compared to the DMD. The DMD layers exhibit higher hardness values compared to the PTA layer (300–315 HV and 320–350 HV, respectively) due to the smaller grain size. The tensile properties of the hybrid PTA-DMD layers are more comparable with PTA layer. The mean yield strengths of samples fabricated with the hybrid PTA-DMD layers are 800–850 MPa, while these properties are 794 MPa, and 984 MPa in samples made with PTA and DMD, respectively.

Keywords Direct metal deposition · Hybrid additive manufacturing · Plasma transfer arc welding · High deposition rate additive manufacturing

1 Introduction

High productivity and quality issues for additive manufacturing (AM) have become increasingly important for the fabrication of large metallic components in recent years. Among several technologies for AM of metallic parts, as reviewed and summarized by Ngo et al. [1], the specification of some of them is desirable to be particularly employed for the production of large structural components. For instance, wire-based electron beam additive manufacturing (EBAM) or wire arc additive manufacturing (WAAM) have a distinct advantage of high build-up rate and is well suited for manufacturing parts of high deposition rate and

✉ M. Dalaee
Dalaee@inspire.ethz.ch

F. Cheaitani
F.Cheaitani@stellba.ch

A. Arabi-Hashemi
ariyan.arabi-hashemi@empa.ch

C. Rohrer
Christian.Rohrer@empa.ch

B. Weisse
Bernhard.Weisse@empa.ch

C. Leinenbach
christian.leinenbach@empa.ch

K. Wegener
wegener@iwf.mavt.ethz.ch

[1] Institute of Machine Tools & Manufacturing (IWF), ETH Zürich, Zürich, Switzerland

[2] inspire AG, Zürich, Switzerland

[3] Stellba AG, Dottikon, Switzerland

[4] Empa, Swiss Federal Laboratories for Materials Science and Technology, Dübendorf, Switzerland

large volumes. However, the fabricated product is limited by available wire materials, the low geometrical accuracy, and the need for a vacuum chamber in case of EBAM.

Blown powder AM utilizes powder as feedstock and provides an advantage of the wide range of material selection. For instance, laser direct metal deposition (DMD) is capable of building complex and precise layers [2]. Nevertheless, the typical productivity rate of the DMD process is not sufficient for meter-size components fabrication. Purchasing a high-power laser source, which can lead to a higher deposition rate, is currently very costly. Plasma transfer arc welding (PTA) is a well-known technology for coating applications. It might be capable of being employed in large volume AM due to the high build-up rate. Regular current PTA enables high powder deposit rates of typically 2–10 kg/h and even higher in high power PTA [3]. Nevertheless, the typical bead width for regular PTA (100–300 A) is 2–40 mm, mostly around 10 mm, which restrict the deposition of small and complex features and require subsequent machining of the built part.

Therefore, it might be challenging to fulfill both high built-up rates and thin and complex elements when fabricating parts for heavy industry applications. Hybrid additive manufacturing (H-AM) has been recently considered as a solution for improving the part quality, functionality, and productivity by assisting or combining two or more technologies as several of them were presented and discussed in the study of Sealy et al. [4]. For instance, Shi et al. [5] investigated in a combination of SLM and WAAM to obtain complex and large part fabrication. In their research, complicated features of a component are fabricated by the SLM technique. In the following, they used the fabricated elements as substrates and completed the rest of the element by WAAM. Qian et al. [6] proposed hybrid plasma-laser deposition manufacturing (PLDM) technology in which an assisting laser beam is introduced into the plasma arc beam to decrease the melt pool diameter and to improve the plasma arc stability. They observed improvement in geometrical accuracy of deposited layers with this technique. In another work, Stempfer [7] applied a hybrid PTA wire-feeding method to increase the deposition rate by employing two gas-transferred arcs. The first PTA torch is used for preheating and forming a molten pool in the deposition area on the substrate, whereas the second PTA torch is applied to melt the wire feedstock. Merklein et al. [8] reviewed the combination of AM into the production chain of conventional manufacturing such as milling or sheet metal forming, which is also part of the recent research to improve accuracy and productivity.

It is believed that the H-AM technique—either a cyclic process chain or simultaneous processes—can further increase the utilization ratio of materials and improve production speed and dimensional resolution and accuracy. Nevertheless, H-AM technology is still facing challenges like the high complexity level of the hybrid solution or multi-sequence of fabrication steps in different workstations. There are unique specification similarities between PTA and DMD techniques explained in the following chapter that motivated authors to investigate the feasibility of a combined DMD-PTA technique. This study analyzes the capability of the contribution of both PTA and DMD methods in a single operating system in order to enhance AM of complex and large components with a high productivity rate. Therefore, this newly proposed manufacturing method can yield the opportunity of three-dimensional deposition with high productivity, dimensional accuracy, and relatively low complexity and costs of equipment. The proposed system can provide a new direction for producing large and complex components. For this purpose, first, the specification of both techniques is discussed to evaluate the capability of their integration in a single operating system. Secondly, samples are fabricated to examine the deposition rate and joining strategy of dissimilar layers. Finally, the microstructure and mechanical properties of the produced samples are analyzed.

2 Specification evaluation for PTA-DMD combination capability

DMD utilizes a laser beam as a heat source to melt the substrate and blown powder materials. The laser beam can be focused and moved with high precision and geometrical flexibility [9]. In PTA, an electric arc is formed between a non-consumable tungsten electrode and a copper nozzle. This is called "pilot arc." Next, the arc is transferred from the orifice to the substrate by feeding plasma gas into the "pilot arc" generating a plasma beam. Metal powder is fed into the collimated plasma beam creating a melt pool of the added material and the substrate material [3, 10].

Technically, there are many similarities in the hardware specifications of the PTA and DMD process. First of all, the PTA torch—similar to the DMD laser nozzle—can be easily mounted to a robot or CNC machine, providing higher freedom of movement during deposition and can thus be used for complex shapes. In addition, the source of energy, which is an electric current in PTA and a laser beam in DMD, can be delivered effortlessly to the process nozzles via cable and optical fiber, respectively. In particular, PTA equipment is comparably less expensive and with a lower level of complexity compared to the DMD technique.

Moreover, there is a close similarity in the suitable powder feedstock morphology and particle size distribution in both processes. The suitable grain size of powders for both processing can be in a range of 50–150 μm according to [3, 9]. The powder is delivered to the coaxial nozzles typically by argon gas flowing with a rate of 3–10 (l/min). This technical similarity ensures employing one powder-feeding unit, which can deliver powder for both processes.

PTA and DMD processes are substantially similar in clad formation since both methods material is deposited via the formation of a melt pool, which offers excellent flexibility in alloy formation and a wide range of materials selection. The clad width

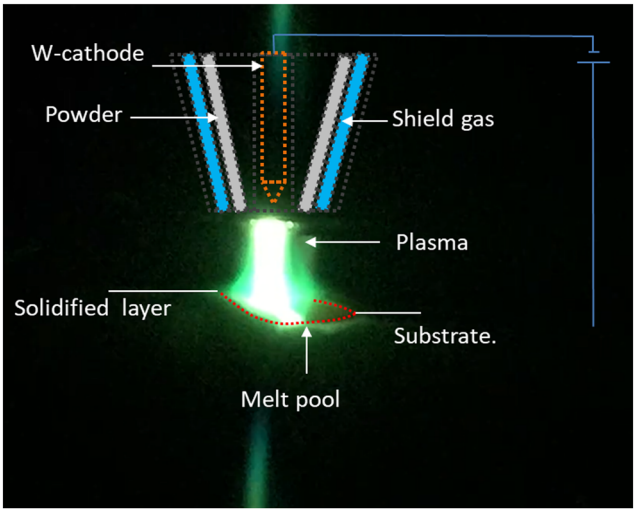

Fig. 1 Photo of plasma and generated melt pool in PTA process. The schematic of the PTA nozzle is shown in the photo. The red-dotted curve shows the melt pool boundary, which is formed during the oscillating of the nozzle

is comparably narrow in the DMD process and mainly specified by the laser spot diameter. PTA is also capable of providing a relatively narrow clad width due to the collimated plasma beam [10]. In micro-PTA, bead widths can be 0.5–3 mm, resulting in deposition rates of 0.1–2 kg/h, according to [3]. This advantage ensures the controllability of the position and excellent shape constancy of the deposited layers, which is crucial in additive manufacturing. Furthermore, the dilution rate of the coated layer is relatively low in both processes. For example, d'Oliveira et al. [11] compared the dilution rate of laser cladding and PTA. When depositing a Co-based alloy, they observed a dilution rate of 6.9% for PTA and 9.4% for laser cladding.

Figure 1 shows a photo of a plasma-generated melt pool in which the schematic of PTA nozzle is illustrated. The photo was taken during an experimental test of this study. As shown in the Figure, the substrate is part of the electric circuit in arc transferred from the torch, and thus, it must consist of an electrically conductive material. The PTA torch can have an additional oscillatory movement perpendicular to the substrate movement [12]. Therefore, the melt pool size is wider than the plasma zone, as shown by a red-dotted line in Fig. 1, which allows limiting the local heat flux and producing flatter beads. As a result, the PTA clad width is relatively wider than DMD clad widths in one pass, which constraints building of small or thin features. However, in low current PTA, there is frequently no oscillation applied, in which electric current for transferred plasma and powder feed rate are relatively low. It allows the deposition of layers with small bead widths as it was examined by Shubert [13]. They described a micro-PTA process in which a bead was deposited as thin as 0.5 mm.

The regular PTA process is a high-temperature process compared to the DMD process, leading to a more pronounced heat penetration into the layer underneath. Therefore, the heat-affected zone (HAZ) is comparably large. The resulting high residual stresses may lead to warpage or deterioration of the mechanical properties of the bulk material, particularly in small components. A fine microstructure can be achieved due to the high cooling rate in both processes. However, the cooling rate is lower in PTA due to the thicker and wider melt pool volume [14]. Moreover, the coating quality is less sensitive to the torch–substrate distance in PTA [3] compared to the DMD process, in which working distance needs to be set accurately for a given laser spot size.

Deposition of layers by PTA on a non-horizontal surface is challenging due to the gravitational acceleration effect on the melt pool. As reported in the study of Wilden et al. [15], a non-horizontal substrate leads to difficulties in handling the melt pool and the flow of the molten material. The authors presented the need for a reduced energy input per unit length by increasing the processing speed or arc power. This effect is much lower or even negligible in DMD due to smaller melt pool and faster solidification.

A comparison of the PTA and DMD process specifications is given in Table 1. The main conclusion of the

Table 1 Comparison of PTA and DMD process specification, according to the discussion given in [3, 9]

Specification	Regular PTA (100–300 A)	Regular DMD (1–4 kW)
Particle size	50–200 μm	50-150 μm
Alloy formation	Melt pool	Melt pool
Substrate	Conductive	Conductive and non-conductive
Multiple powders	Yes	Yes
Powder carrier gas	Argon	Argon
Working distance	Less sensitive	High sensitive
Atmosphere protection	Shield gas	Shield gas
Automation level	High	High
Heat-affected zone (HAZ)	High	Low
Fabrication of complex part	Limited	Advantage
Bead geometry	2–40 mm	1–4 mm
Deposition rate	2–10 kg/h	0.5–3 kg/h

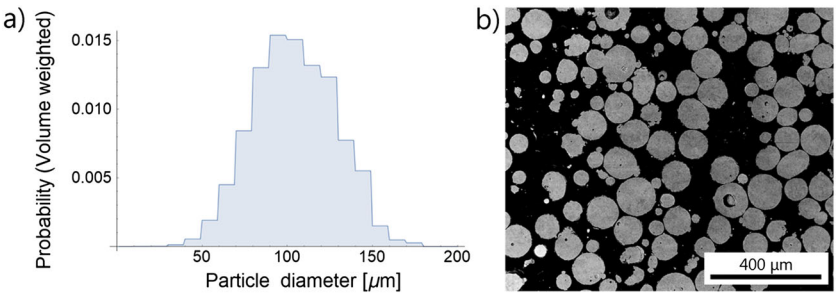

Fig. 2 Measurement result of powder stainless steel EN X3CrNiMo13-4, **a** powder size distribution and **b** SEM image of powders cross-section

discussion is that both PTA and DMD processes are capable of being integrated into one operating system. It is more technical effortless to design a system with an automatic tool changer for individual PTA and DMD deposition nozzle. PTA head due to the higher deposition rate beneficiary can fabricate less precise and thick elements whereas complex and thin features of the component can be built by the DMD process. In the following chapters, the layer-wise contribution of PTA and DMD in the fabrication of samples is investigated to analyze productivity, process stability, metallurgical quality, and mechanical properties of the combined layer. The detailed experimental approach includes materials, process parameters and setups, testing methods, and experimental protocols.

3 Materials and experimental details

3.1 Materials

Stainless steel EN X3CrNiMo13-4 was used as powder feedstock and substrate for the deposition of layers in both PTA and DMD process. The powder particles had a size of 63–150 μm. The average powder diameter was 104 μm (cf. Fig. 2a). The powder particles appeared to be spherical and can be described as dense, although microscopic pores were occasionally observed, as shown in the scanning electron microscopic (SEM) image in Fig. 2b. Round plates with a diameter of 200 mm and thickness of 30 mm and round shafts with a 100-mm diameter and a 100-mm length were used as substrates in the experiments.

3.2 PTA specification and setup

The PTA machine used in this work has a rotary tilted table and a column-boom axis type shown in Fig. 3. The maximum current output of power source is 400 A. A KENNAMETAL IPM 250 torch with a two-beam powder nozzle and a maximum powder feed rate of 80 g/min was employed.

Three samples were produced with different powder feed rates, scan speed, and electric current in order to define the suitable parameters for processing of EN X3CrNiMo13-4. The most suitable parameters are selected after cross-sections analysis of the samples considering deposition rate and metallurgical bonding. These parameters are listed in Table 2. The parameters, which were used for productivity evaluation with 240 A

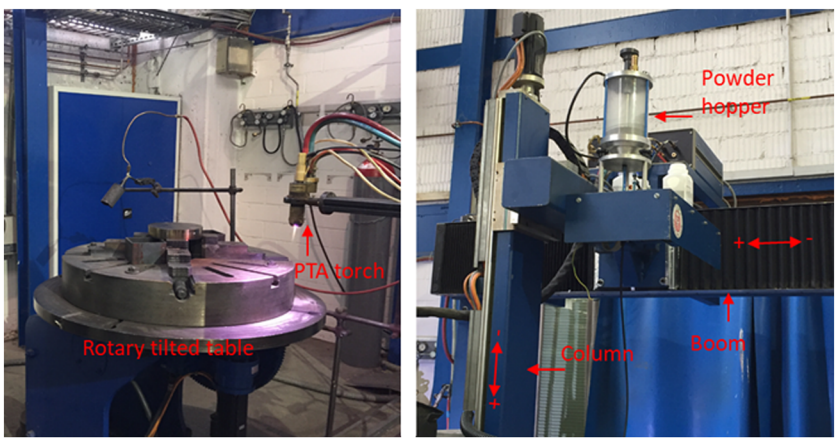

Fig. 3 PTA machine units: left figure shows PTA torch and rotary tilted table. Right figure shows torch manipulator (column and boom) and powder hopper

Table 2 Main parameters of the PTA process

Process parameters	Condition 1	Condition 2
Current (A)	240	120
Oscillation speed (mm/min)	700	700
Travel speed (mm/min)	140	80
Oscillation distance (mm)	22	16
Powder feed rate (g/min)	50	22
Pilot gas flow rate (l/min)	3	3
Shield gas flow rate (l/min)	18	18
Working distance (mm)	12	12

and 120 A are designated as condition 1 and condition 2, respectively. In a pulsed current PTA test, the powder feed rate of 22 g/min and pulse length of 0.5 s was applied.

3.3 DMD specification and setup

The DMD process was carried out on a CNC–DMD machine using a diode laser with a wavelength of 1064 nm, and a coaxial three-jet powder beam nozzles at the working distance of 12 mm. Argon gas was used for shielding and powder delivery. Three samples were produced with different powder feed rates, scan speed, and laser power. The most suitable parameters were selected after cross-section analysis of samples considering the maximum clad height and metallurgical quality. The main DMD process parameters are given in Table 3.

3.4 Characterization and testing methods

The clad geometries and grain structures of samples were studied using a Keyence VHM 5000 optical microscope after the proper etching process, as shown in Table 4. A further microstructural examination is performed on samples with a FEI Nova Nano SEM 230 device and using a backscattered electron detector. The surface roughness of the samples perpendicular to the track path is measured by a 3D optical image made by ALICONA infinite focus G4 microscope. XRD measurements were done on a Bruker D8 diffractometer using CuKalpha radiation to identify the phases present in the material. Diffracted x-rays were collected by a 1D Lynxeye detector.

Table 3 Main parameters of the DMD process

Laser power (W)	Powder feed rate (g/min)	Track overlap (%)	Scan speed (mm/min)	Shield gas flow rate (l/min)	Carrier gas flow rate (l/min)	Spot diameter (mm)
2400	14.5	50	1000	5	4	3.5

Table 4 Etching solution and procedure used in metallography of samples

Etchant solution	Description
Adler etchant	Hydrochloric acid 150 ml, ammonium copper chloride 9 g
Etching time	1-min immersion at room temperature

Tensile properties and hardness are measured to evaluate the mechanical properties of combined PTA and DMD layers. “Dog bone-shaped” flat test specimens (according to DIN50125 2016 type E) were prepared from samples, machined with an electro-discharge wire cut machine, as shown in Fig. 6a. Two test specimens were prepared from each sample. Tensile tests were carried out according to EN ISO 6892-1:2017 using a 600 kN universal test machine of type Zwick 1494 with a 10 kN load cell of type HBM U2AK and a clip-on extensometer of type MINI MFA 2 as shown in Fig. 6b.

Microhardness tests are carried out with Qness Q10m machine, using two types of Vickers indenter HV 5 and HV 0.5 due to variation in grain sizes of samples. Measurement distance over the cross-section is 0.25 mm and 0.5 mm for HV 0.5 and HV 5, respectively.

3.5 Experimental protocols

The experiments were carried out in three steps.

In the first step, the clad geometry and the productivity of both processes were examined by fabricating single tracks using the parameters listed in Table 2 and Table 3. The deposition rate was calculated according to the following formula.

$$\dot{D} = v \times \ A \times \rho \tag{1}$$

with $\dot{D}$, deposition rate; v,scan speed; A, the cross-section area of bead; and ρ, the density of stainless steel. The powder melting efficiency was calculated considering the obtained deposition rate and the powder mass flow through

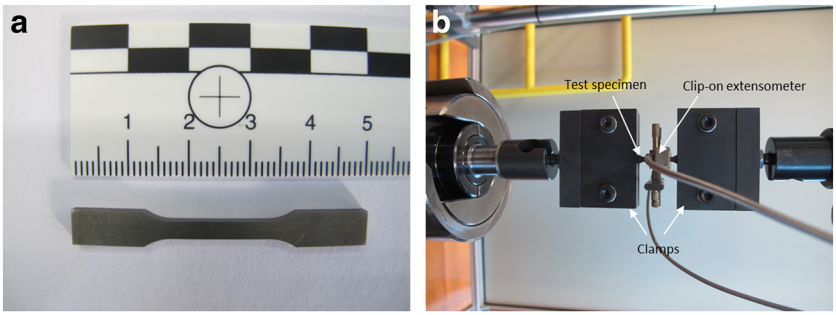

Fig. 4 **a** "Dog bone-shaped" flat test specimen prepared with wire cut machine for tensile test. **b** Tensile test setup using a 600-kN universal test facility

the nozzles.

In the second step, experimental tests were performed with four cylindrical solid rods to characterize the microstructure and mechanical properties of the samples produced by combined PTA–DMD deposition.

In total, four samples were produced.

•N.1: first layer by PTA and second layer by PTA
•N.2: first layer by DMD and second layer PTA
•N.3: first layer by DMD and second layer by DMD
•N.4: first layer by PTA and second layer by DMD

This experiment represents the conditions, which can occur during a layer-wise combined PTA–DMD fabrication of a component. During sample manufacturing, the powder was continuously deposited onto a rotating rod, and the deposition head in both DMD and PTA was moved along the rod axis. The deposition condition of the DMD process on the PTA layer underneath was monitored with video cameras shown in Fig. 5 (left). No noticeable event in the DMD process, such as a large amount of spatter or process light flashing was realized during monitoring. Figure 5 (right) shows the schematic of build-up direction and orientations of hybrid PTA-DMD layers, referred to sample N.4.

A heat treatment at 550 °C for 2 h with slow cooling was applied to all samples N.1–4 after the deposition to relief thermal residual stresses before metallographic preparation. Liquid penetrant non-destructive testing was used on the layers to detect any surface defect. All test pieces N.1–4 are longitudinally and transversely cross-sectioned and polished for metallography. Besides, the surface layer of samples was sectioned to examine the microstructure of the upper layer of the sample. Three samples from each test pieces are prepared in order to check the repeatability of the analysis.

In the third step, the contribution of both processes in the building of part was examined. Small elements were fabricated by the DMD, and broad and flat features were deposited by the PTA in order to decrease the overall built-up cycle. For this purpose, a simple

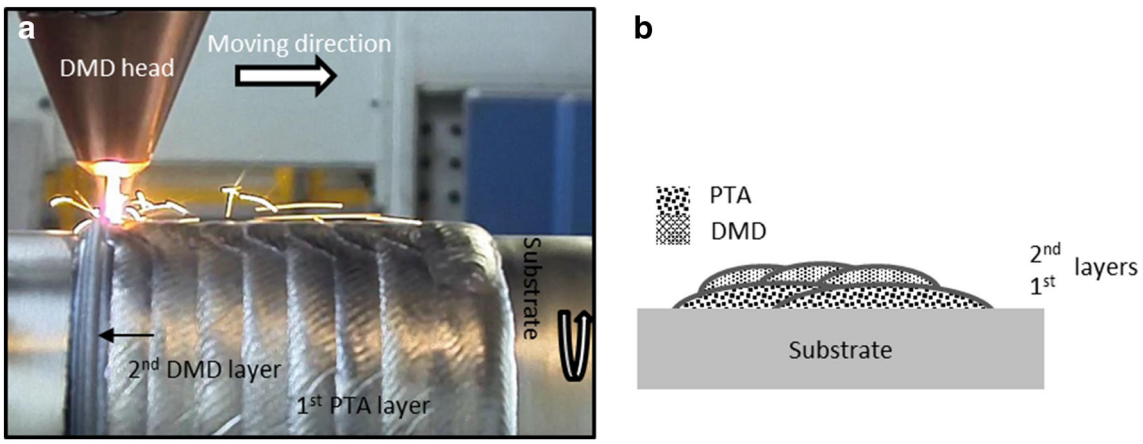

Fig. 5 Deposition of hybrid layers onto a rotating substrate. Panel **a** shows the laser DMD process, depositing the second layer on the first PTA layer underneath. Panel **b** shows the schematic of the built-up direction of the sample with hybrid PTA-DMD layers (referred to the sample N.4)

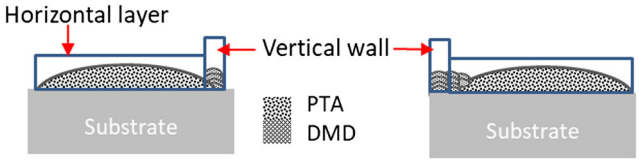

Fig. 6 Side deposition approaches in combined PTA and DMD fabrication. On the left, first, the vertical wall is fabricated by DMD, and then the PTA track is deposited next to the wall. In the right, the PTA layer was deposited first, and then DMD tracks build up the vertical wall and complete the gap between the two tracks

part consisting of one horizontal layer and a vertical wall next to it was designed, as shown in Fig. 4. SKM–DCAM software was used to generate toolpath in building of the parts. Two approaches were considered to produce this part. In the first approach, the wall is fabricated by DMD, and after that, the PTA track is deposited next to the wall as a horizontal layer (Fig. 6, left). In the second approach, the PTA layer was deposited first, and then DMD tracks were deposited next to it to build up the vertical wall and complete the gap between the two tracks (Fig. 6, right).

4 Results and discussion

4.1 Clad geometry and deposition rate

Table 5 summarizes the single track geometries as well as the deposition rates of samples fabricated in the first experiment. The deposition rate in the PTA (120 A) process is twice as high as that during DMD. By doubling the transferred arc current to 240 A, a higher powder feed rate was applied, resulting in an increase of the deposition rate approximately by a factor of two. The powder melting efficiency is high in the PTA compared to the DMD and reached 92% in PTA (240 A). The bead geometry is both broader and thicker in the PTA samples than for the DMD samples. A smaller clad width was obtained with pulsed-PTA, which offers the advantage of the fabrication of thin elements of the part without changing the PTA torch. However, the deposition rate decreased by 32% due to lower powder catchment efficiency.

When comparing the etched cross-sections of oscillating PTA and pulsed-PTA coatings, as shown in Fig. 7, one can observe a higher melt pool depth in pulsed-PTA. Furthermore, penetration is more focused in the middle of the track in puled-PTA (Fig. 7b) while flatter clad and uniform metallurgical bonding to the substrate was obtained in oscillating strategy with the same PTA torch. When comparing the HAZ of the deposition tracks, this factor is significantly higher in the PTA process. Nevertheless, it must be pointed out that to achieve the same track width and height made by PTA (120 A) process, approximately 10 DMD tracks with 50% overlap and 4 increment layers need to be deposited, which may cause pronounced heat accumulation in the part if the length of deposition paths is small, and thus enlarge the HAZ depth.

4.2 Joint layers of PTA and DMD

4.2.1 Surface condition

The surface texture of the samples produced in the second experiment is shown in Fig. 8. DMD surfaces are smoother than the PTA layer due to wider bead width, larger track distance, and nozzle oscillation in the latter case. The red-dotted line shows the track distance of each bead, which has 50% overlap from the sidetrack. The surface roughness Ra and Rz and waviness Wa and Wz of fabricated samples listed in Table 6. The maximum waviness Wz of the PTA layer is approximately 1.7 higher than the DMD layer. In both samples N.3 and N.4, the measured surfaces are DMD, but the layers underneath are dissimilar (DMD and PTA, respectively). However, there are

Table 5 Track geometry, deposition rate, and melting efficiency of single tracks deposited with the PTA and DMD processes

Process parameters	Clad width (mm)	Clad height (mm)	HAZ depth (mm)	Deposition rate (kg/h)	Powder melting efficiency (%)
DMD	3.38	0.54	1.07	0.54	64.3
PTA (120 A)	16.37	2.37	8.75	1.13	85.6
PTA (120 A) pulsed	11	3.5	10	0.77	58.3
PTA (240 A)	22.19	2.75	> 12	2.76	92

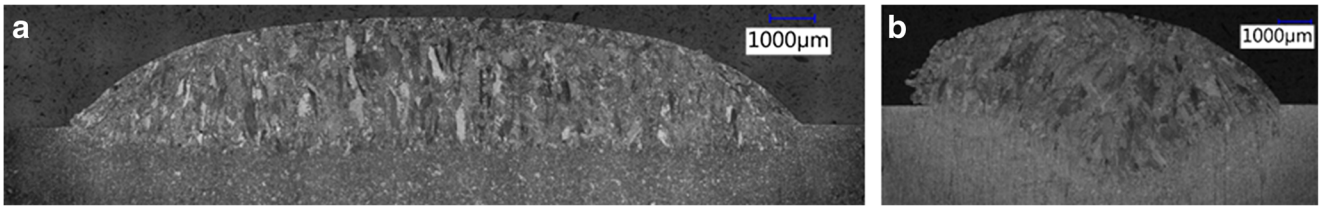

Fig. 7 Optical images of the cross-sectioned single tracks deposited with PTA process. **a** 120 A with oscillation of torch. **b** Pulsed-PTA 120 A, pulse duration 0.5 s, without oscillation of torch. Samples etched with Adler's solution

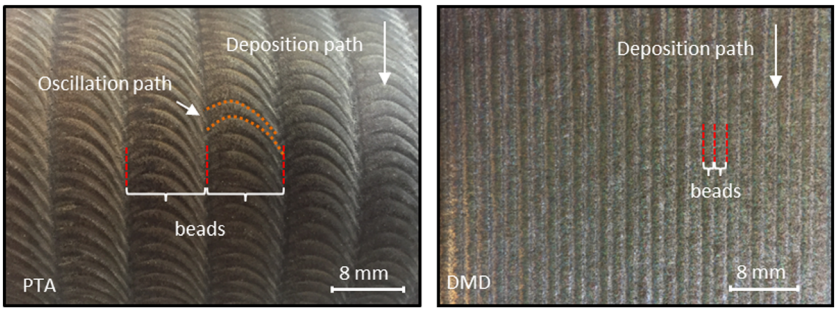

Fig. 8 Surface texture of the upper layer of fabricated samples with PTA and DMD process from EN X3CrNiMo13-4 powder material. PTA Surface (left) is rougher compared to DMD layer (right) due to the oscillating path and larger track distance

slight variations in surface roughness and waviness between these samples.

4.2.2 Side deposition of PTA and DMD layer

In the following, the results of the side deposition of PTA and DMD tracks fabricated according to the third experimental step were discussed. In the first approach, a DMD contour wall with a 4-mm thickness was built in which the flat area was deposited with 2-mm DMD raster layers. Next, a PTA single track is built on the side of a DMD wall, as shown in Fig. 9. As indicated by a red-dotted line in Fig. 9, the PTA track is not uniformly joint to the side of the wall over the path line and led to excess or insufficient melting of the vertical sidewall. This condition may lead to the risk of damage or poor track joint.

Table 6 Surface roughness and waviness value of samples, measured perpendicular to deposition path. The upper layer of samples N.1 and N.2 are PTA layer, and samples N.3 and N.4 are DMD layers

Properties	PTA surface Samples		DMD surface Samples	
Unit [µm]	N.1	N.2	N.3	N.4
Ra	9.48	10.88	4.48	4.71
Rz	70.04	70.34	34.28	35.11
Wa	103.43	101.50	36.10	36.09
Wz	174.94	175.54	98.85	100.25

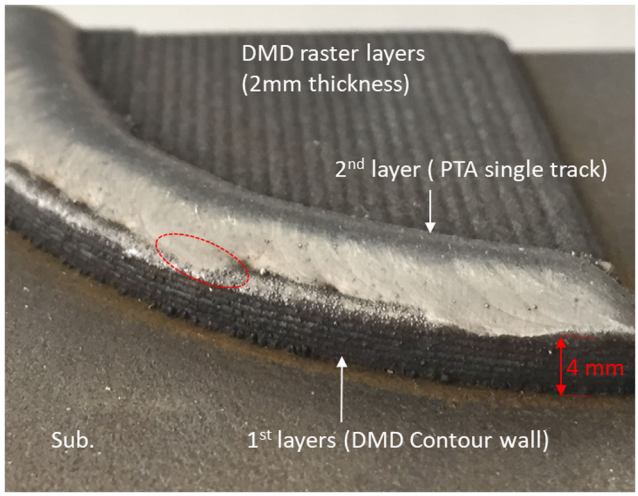

Fig. 9 A single PTA track deposited on the side of the DMD wall, which was deposited with eight incremental layers (first approach). The red-dotted contour shows the excess melting of the vertical DMD wall by the PTA track

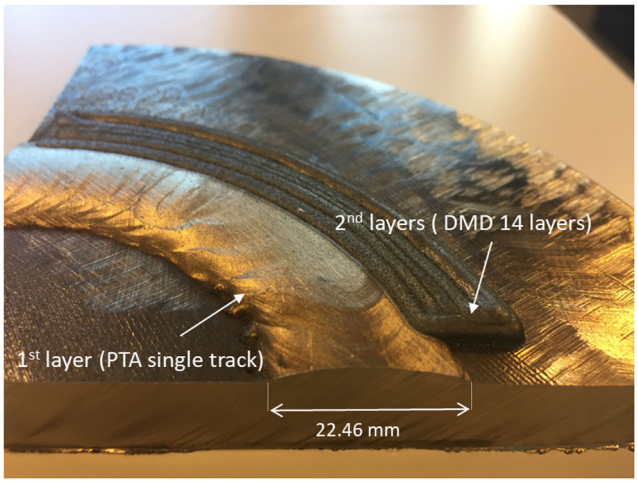

Fig. 10 DMD layers were deposited on the side of a PTA single track (second approach). The gap between the DMD wall and the PTA track was completed with the DMD layers

In the second approach, a PTA track was deposited with 240 A first, and then layers were fabricated by DMD to build a small wall and fill the gap (cf. Fig. 10). The layers were joint uniformly without a visual non-welded zone, although the PTA track width is deviated ± 0.5 mm. However, the sample was cut off in two sections to ensure metallurgical bonding between different layers.

In the cross-sectional micrograph shown in Fig. 11, three zones can be observed. Those are the DMD wall, the single PTA track, and the gap between the DMD layer and the PTA track filled with DMD. A good metallurgical bond was obtained with this strategy. However, a pore-like defect is detected between DMD layers in the intersection gap area caused by insufficient overlap distance (20%) between layers.

Due to the thick bead layer and larger clad angle in the PTA track compared to the DMD track, the generation of the deposition toolpath in this section requires computer-aided manufacturing (CAM) software to determine the suitable track distance and path numbers to fill this zone uniformly with DMD layers. The available CAM software provides selecting layer thickness and size of the bead in each layer, which permits the contribution of both processes during the fabrication of parts. However, CAM tools should calculate the miss-welded materials after a rough deposition step by the PTA process and complete the miss-welded zone with a finishing step using the DMD process.

4.3 Microstructure and mechanical properties of the combined layers

4.3.1 Microstructure and phase constituent

The XRD measurements have been conducted to evaluate the influences of different temperature gradients realized by PTA and DMD on phase formation during solidification. The results shown in Fig. 12 confirms that both DMD and PTA samples are almost entirely martensitic. There are evident diffraction peaks at 2 T 44.5°, 64.7°, 82.0°, and 98.5° at (110), (200), (211), and (220) facets of martensitic phase, respectively. The DMD material exhibits a small phase fraction of residual fcc austenite at $2\theta_{111} = 43.5°$.

PT inspection of all four samples N.1–4 does not reveal any major surface defects on the surfaces of the samples. Microstructure images of cross-sectioned and etched samples are shown in Figs. 13 and 14 in which "C" "L" and "T" stand for transverse, longitudinal, and top directions, respectively. Figure 13 presents a longitudinal section of the samples consisting of three zones:

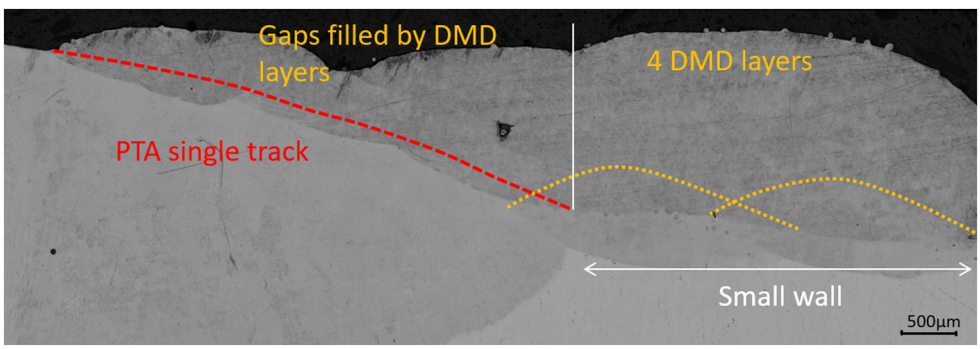

Fig. 11 Cross-sectional micrograph image of side joins of a PTA track and the DMD clads. The orange-dotted contours show the boundaries of the first two DMD beads. Red-dotted contour shows the boundary of the PTA single track

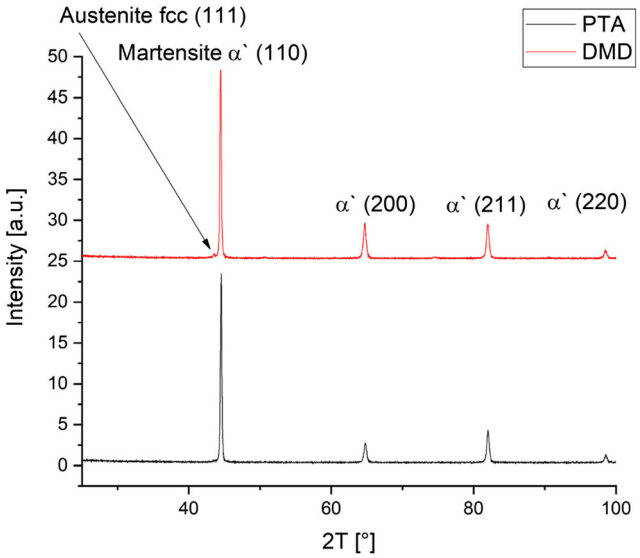

Fig. 12 XRD measurements of the PTA and DMD layers show that both materials are almost entirely martensitic. The DMD material shows a small phase fraction of austenite at $2T_{111} = 43.5°$

DMD zone, PTA zone, and interface zone. Arrow in the optical images (Fig. 13, L-4) depicts the intersection of DMD and PTA layers in sample N.4. No clear intersection was observed between the two PTA layers in sample N.1. This fact may stem from the high thermal load of the PTA plasma, which is like a tempering process and will affect the grain growth in the intersection zone of PTA layers because of recrystallization. In sample N.2, the DMD layer underneath was partially re-molten by the PTA layer above due to the dilution depth of PTA. The red-dotted line in the cross-section image shown in Fig. 14, C-2 divides the area of intersection between two layers.

Nevertheless, only a part of the first layer remained un-molten. This pattern is observed in all cross-section zones of sample N.2. Grains are significantly larger in the PTA layer in all three orientations compared with the DMD layer and can reach sizes of 1000–1500 μm as measured by ImageJ software [16]. These large grains are due to the large melt pool size and the corresponding longer melt pool lifetime, leading to more pronounced grain growth.

The SEM micrograph of sample N.4 shows the coarse columnar shape of the martensitic grains in the PTA layer (indicated by the red-dotted line in Fig. 15a). As optical images show good metallurgical bonding between layers, images were taken by SEM to confirm a dense microstructure in individual layers and the intersection zone between dissimilar layers. However, at higher magnification (× 2000), some porosity in the range of 1–1.8 μm is observed in the DMD layer (cf. Fig. 15b).

The pores have been observed not only in the intersection zone but also in all DMD areas with the same distribution, indicating that these porosities are not relevant to the combined process, but it is inherent to the chosen parameters in DMD process as it was also observed in sample N.3. The powder carrier gas and faster solidification of the melt pool in the DMD process presumably play a role in forming these porosities in DMD layer with a higher number compared to PTA layer.

4.3.2 Hardness profiles

Figure 16 shows the hardness distribution across the different layers in all four samples. The hardness values vary from the top layer to the base metal according to the applied process. The range of the hardness of PTA layers and DMD layers is between 300 and 315 HV and 320–350 HV, respectively. The DMD layers exhibit higher hardness values compared to PTA, as shown in Fig. 16c, d. This can be explained with the refined microstructure of the martensitic structure. Comparing the hardness diagrams in Fig. 16a, d, it can be concluded that hardness in the HAZ is in the range of 340–350 HV after applying PTA layer compared to the hardness of 290 HV of the substrate in the center of the sample shown in the Figure. This may be explained with the temperature evolution during the PTA process, which modifies the microstructure of the layer underneath to smaller grain size compared to the bulk metal. Due to the smaller grain size in the DMD layer, more hardness changes interval can be seen with HV0.5 indenter compare to HV5 in the measurement length of 1.75 mm (cf. Fig. 16c).

4.3.3 Tensile property

Figure 17 shows the stress-strain curves for all four samples. Two measurements were performed per sample, and there is a good agreement between both measures. The 0.2% yield strength and the ultimate tensile strength are indicated in the graphs with σ_y and σ_{UTS}, respectively. The average yield strength is 794 MPa, 800 MPa, 984 MPa, and 845 MPa for the samples N.1, N.2, N.3, and N.4, respectively. The average ultimate tensile strength is 855 MPa, 859 MPa, 1034 MPa, and 897 MPa concerning the sample N.1 to N.4. It can be seen that the DMD layers in sample N.3 exhibit

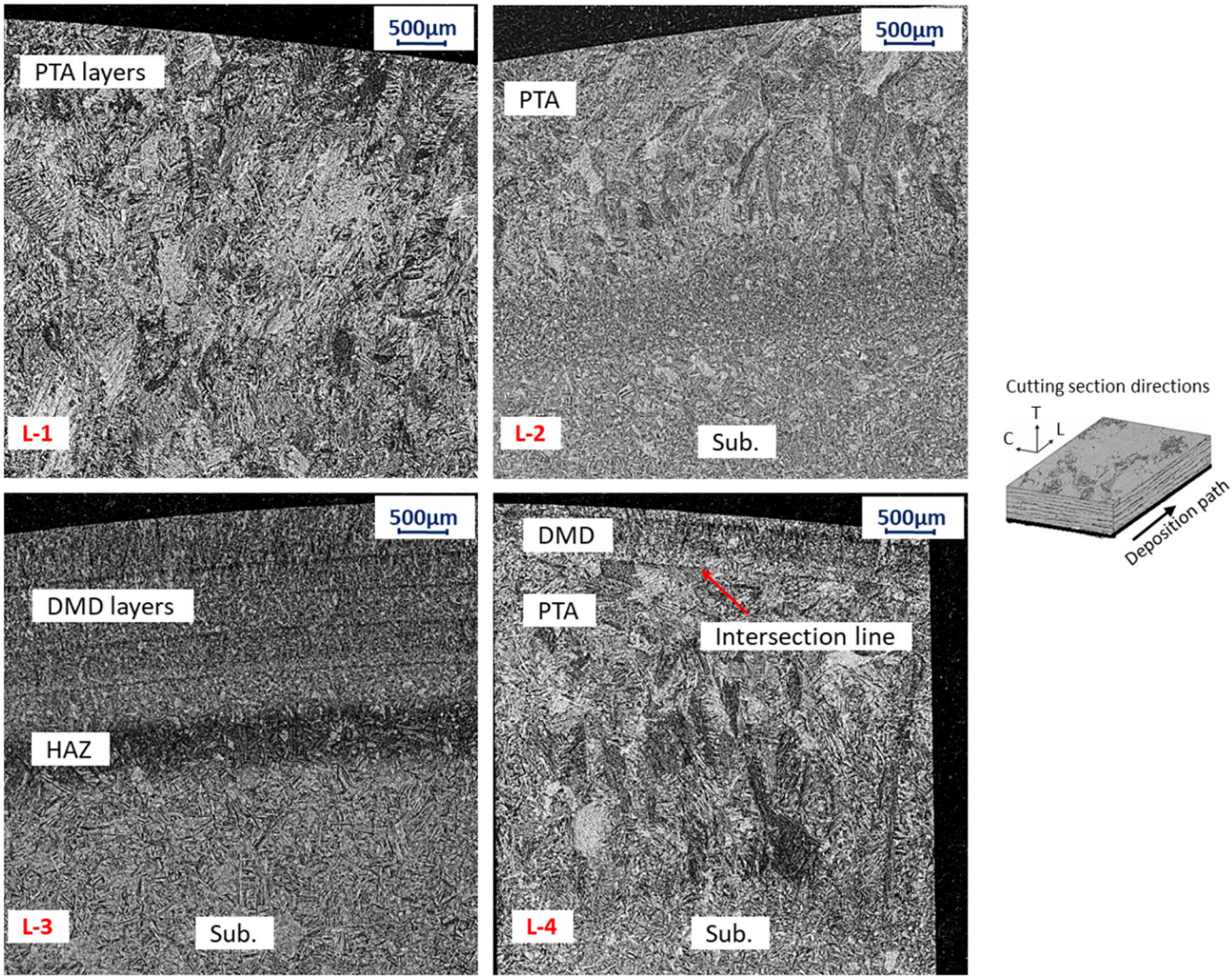

Fig. 13 Optical image of longitudinal sections of samples (stainless steel EN X3CrNiMo13-4), etched with Adler solution. L-1, sample N.1 (PTA + PTA); L-2, sample N.2 (DMD + PTA); L-3, sample N.3 (DMD + DMD); L-4, sample N.4 (PTA + DMD). Arrow in Fig. L-4 shows the intersection of DMD and PTA layers

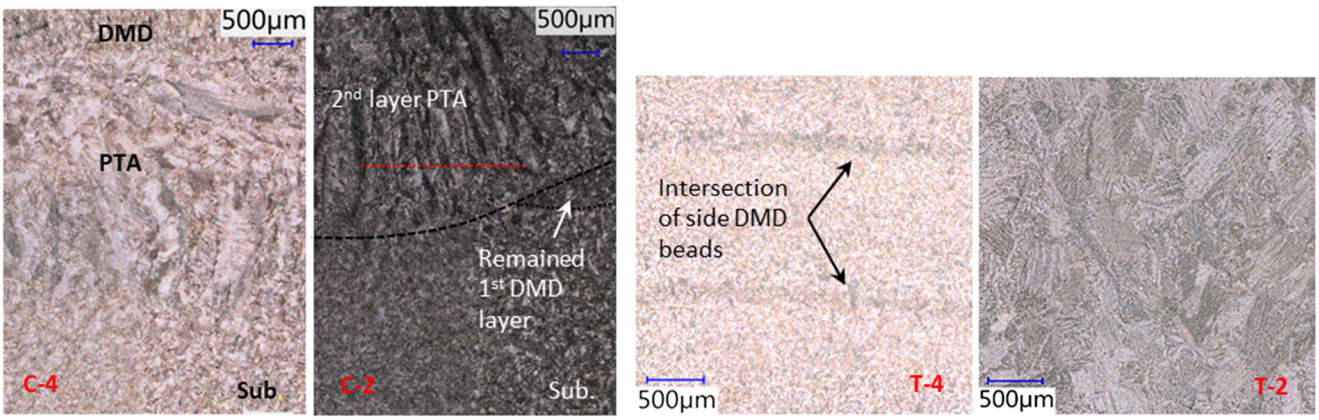

Fig. 14 Optical image of transverse section and upper layer of samples N.4 and N.2, etched with Adler solution. C-4 and C-2 transverse section of sample N.4 (PTA + DMD) and sample N.2 (PTA + DMD), respectively. The red-dotted line divides the area between 1st DMD layer and 2nd PTA layer during deposition, which DMD layer was molten partially by PTA process. Black-dotted lines show the boundaries of layers. T-4 and T-2 show the upper layer of samples N.4 and sample N.2, respectively

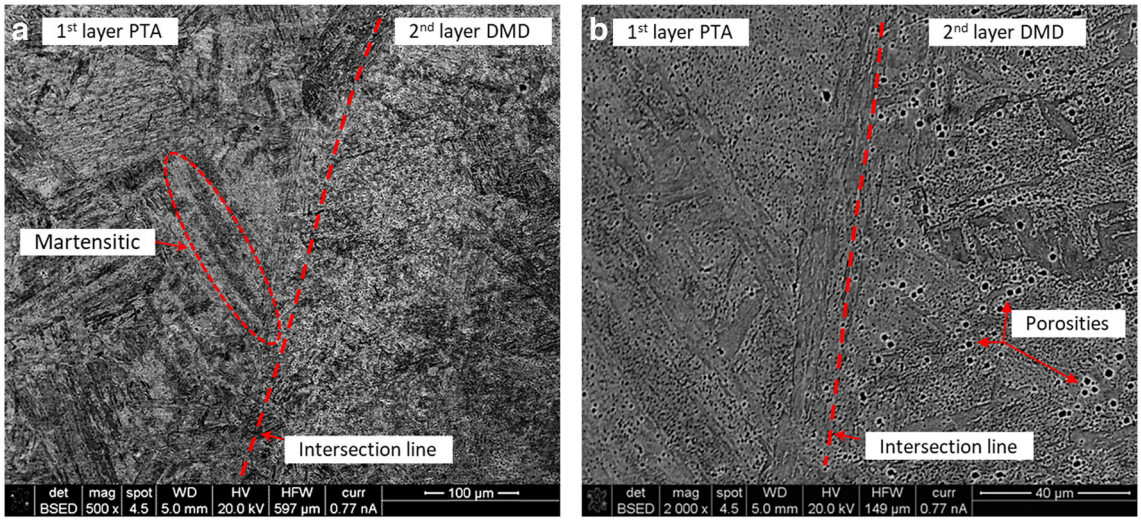

Fig. 15 SEM micrograph of the intersection zone of PTA-DMD in the cross-sectioned sample N.4. **a** × 500 and **b** × 2000 magnitude. The coarse columnar shape of the martensitic grains in the PTA layer is shown in the red-dotted curve. Porosities in the range of 1–1.8 µm in the DMD zone are shown by arrows

approximately 20% higher tensile strength than those of PTA layers in sample N.1. The higher yield strength in the DMD process can be related to the grain size. The larger grain size of the PTA discussed in chapter 4-4, leads to lower yield strength according to the Hall–Petch relationship as well as to higher elongation at fracture. In combined layers of PTA and DMD, samples N.2 exhibit a slightly increased tensile strength than sample N.1.

This is assumed to be due to the partial re-melting of the DMD layer during the PTA process, as it was discussed in chapter 4.3. In fact, the examined specimen mainly consists of the PTA layers. On the other hand, a hybrid PTA-DMD sample (N.4) has around 5% higher tensile strength than samples N.1 due to the addition of the DMD layers, which affect the overall tensile properties. The specimen N.4 contains nearly equal thickness of the PTA and DMD layer. The results indicate that the tensile properties of the hybrid layers are more comparable with PTA layer properties.

5 Conclusion and outlook

In this study, the capability of integration of the PTA-DMD process was analyzed by specification evaluation, fabrication of samples from material stainless steel EN X3CrNiMo13-4, and microstructure and mechanical properties analysis of combined layers. The following conclusion can be drawn.

- Specification comparison between PTA and DMD techniques indicates the capability of designing a combined PTA-DMD process with a low level of complexity and cost. This process may combine the advantages of high deposition rates and high-dimensional resolution during fabrication.
- The proposed operating system can be equipped with individual PTA and DMD head and would be able to fabricate large and complex components with high productivity. During the fabrication, the PTA nozzle can be loaded for building up of the large-size elements due to the thick and wide layers, and DMD can be employed in completing the component by deposition of elements with higher complexity, smaller feature size, and higher dimensional accuracy.
- Technically, both techniques provide low dilution rates, but when they are compared, PTA generally has a higher melting depth than DMD due to its higher heat input, which also larger HAZ.
- Side-by-side deposition of layers by PTA and DMD is challenging due to the clad geometry differences and the high thermal load of PTA, which may cause excess or insufficient deposition. A strategy in which layers are built first by PTA and then DMD is used to complete the rest of the part leads to good side-bonding quality of dissimilar layers with minimal risk of damaging small geometrical elements by PTA. However, further research on side-by-side deposition and CAM strategy would be required to provide a possibility of the contribution of both processes in each individual layer.

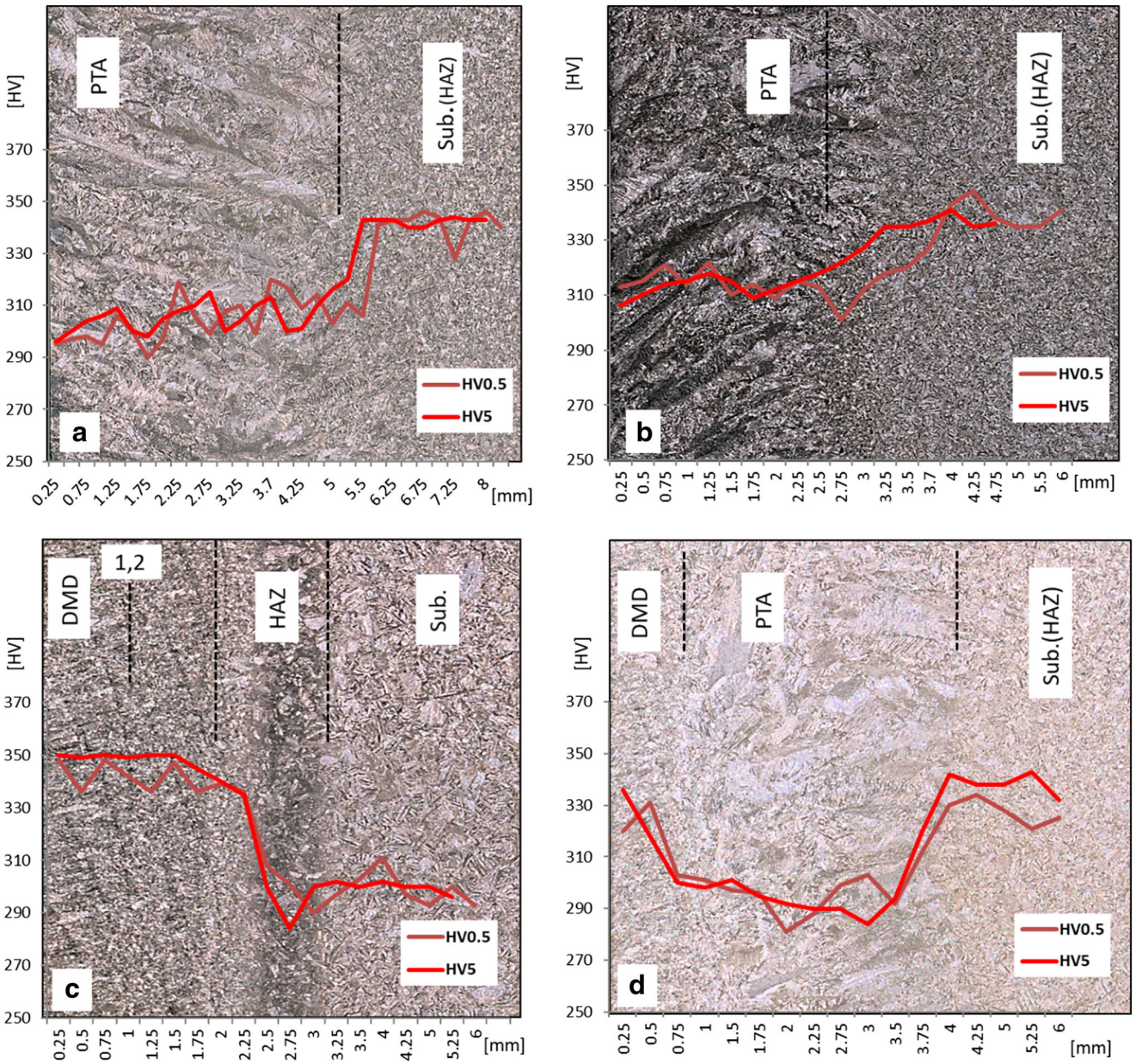

Fig. 16 Results of microhardness of cross-sectioned samples, measured with HV0.5 and HV5 indenters. **a** Sample N.1 (PTA + PTA); **b** samples N.2 (DMD + PTA); **c** samples N.3 (DMD + DMD); **d** Sample N.4 (DMD + PTA)

- Both DMD and PTA samples present almost entirely martensitic. PTA layers present coarse columnar martensitic grains compared to the fine grain of the DMD layer. The grain size difference between layers led to mechanical properties variation. DMD coatings have a higher hardness and strength than PTA layers and the bulk material. The tensile properties of hybrid DMD–PTA layers are more comparable with the ones of PTA layers. The mean yield strengths of samples fabricated with the hybrid PTA–DMD layers are 800–850 MPa, while these properties are 794 MPa and 984 MPa in samples made with pure PTA and pure DMD, respectively.

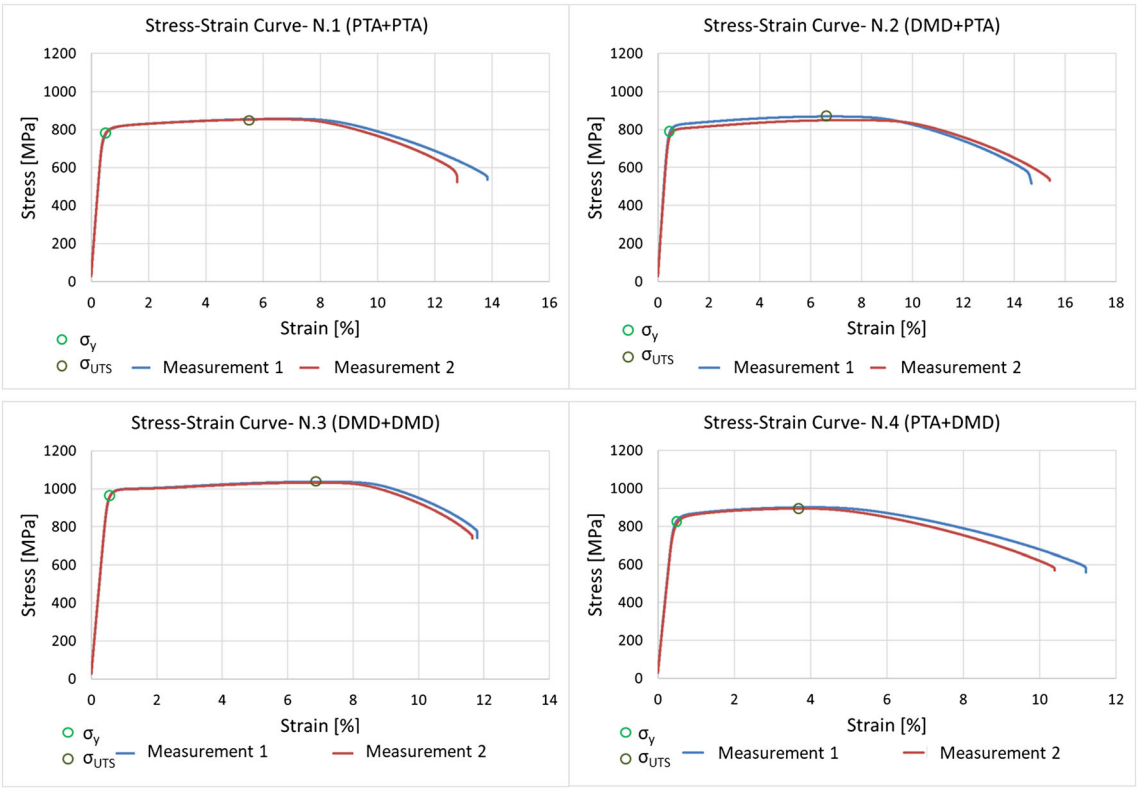

Fig. 17 Tensile properties of samples N.1-N.4. Measurement 1 and measurement 2 shows the results of two "dog bone-shaped" flat specimen from each sample. σ_y and σ_{UTS} are 0.2% yield strength and the ultimate tensile strength, respectively

Acknowledgments The authors would like to sincerely acknowledge Mr. Philipp Jutzi from Stellba AG for the generous support in providing the machines to carry out part of the experimental test in Stellba AG as well as Mr. Andreas Gisler and Milos Radujkov for their help in performing the experiment. We would also like to extend thanks to Mr. Matthias Pfister from Burckhardt Compression AG for materials supplied and Mr. Knut Krieger from inspire AG for the metallography of required samples.

Funding information This work was financially sponsored by the Swiss innovation agency Innosuisse (Grant No. 27436.1 PFNM–NM), which is gratefully acknowledged.

References

1. Ngo TD, Kashani A, Imbalzano G, Nguyen KTQ, Hui D (2018) Additive manufacturing (3D printing): a review of materials, methods, applications and challenges. Compos Part B 143:172–196. https://doi.org/10.1016/j.compositesb.2018.02.012
2. Weng F, Gao S, Jiang J, Wang J, Guo P (2019) A novel strategy to fabricate thin 316L stainless steel rods by continuous directed energy deposition in Z direction. Addit Manuf 27:474–481
3. Fauchais PL, V.R. Joachim Heberlein, Maher I. Boulos (2014) Thermal spray fundamentals: from powder to part. Springer US,
4. Sealy MP, Madireddy G, Williams RE, Rao P, Toursangsaraki M (2018) Hybrid processes in additive manufacturing. Journal of Manufacturing Science and Engineering 140 (6):060801-060801-060813. doi:https://doi.org/10.1115/1.4038644
5. Shia X, Maa S, Liua C, Wua Q, Lua J, Liub Y, Shib W (2017) Selective laser melting-wire arc additive manufacturing hybrid fabrication of Ti-6Al-4V alloy: microstructure and mechanical properties. Mater Sci Eng A 684:196–204. https://doi.org/10.1016/j.msea.2016.12.065
6. Qian Y-P, Huang J-H, Zhang H-O, Wang G-L (2008) Direct rapid high-temperature alloy prototyping by hybrid plasma-laser technology. J Mater Process Technol 208(1):99–104. https://doi.org/10.1016/j.jmatprotec.2007.12.116
7. Stempfer F (2014) Method and arrangement for building metallic objects by solid freeform fabrication
8. Merklein M, Junker D, Schaub A, Neubauer F (2016) Hybrid additive manufacturing technologies – an analysis regarding potentials and applications. Phys Procedia 83:549–559. https://doi.org/10.1016/j.phpro.2016.08.057
9. Toyserkani E, Khajepour A, Corbin SF (2004) Laser cladding. CRC Press
10. Gatto A, Bassoli E, Fornari M (2004) Plasma Transferred Arc deposition of powdered high performances alloys: process parameters optimisation as a function of alloy and geometrical configuration. Surf Coat Technol 187(2):265–271. https://doi.org/10.1016/j.surfcoat.2004.02.013
11. d'Oliveira ASCM, Vilar R, Feder CG (2002) High temperature behaviour of plasma transferred arc and laser Co-based alloy coatings. Appl Surf Sci 201(1):154–160. https://doi.org/10.1016/S0169-4332(02)00621-9
12. Hunt CS (1988) Plasma transferred arc (PTA) surfacing of small and medium scale components – a review. Welding Institute Members Report 364/1988

13. Shubert GC (1987) Welding apparatus method for depositing wear surfacing material and a substrate having a weld bead thereon. Google Patents,
14. Oberländer BC, Lugscheider E (1992) Comparison of properties of coatings produced by laser cladding and conventional methods. Mater Sci Technol 8(8):657–665. https://doi.org/10.1179/mst.1992.8.8.657
15. Wilden J, Bergmann JP, Frank H (2006) Plasma transferred arc welding—modeling and experimental optimization. J Therm Spray Technol 15(4):779–784. https://doi.org/10.1361/105996306x146767
16. ImageJ Fiji. https://imagej.net/Fiji